



## Article

# SiON<sub>x</sub> Coating Regulates Mesenchymal Stem Cell Antioxidant Capacity via Nuclear Erythroid Factor 2 Activity under Toxic Oxidative Stress Conditions

Neelam Ahuja<sup>1,†</sup>, Kamal Awad<sup>1,2,\*,†</sup> , Su Yang<sup>3</sup> , Antonios Mikos<sup>4</sup>, Pranesh Aswath<sup>2</sup> , Simon Young<sup>5</sup> , Marco Brotto<sup>1</sup> and Venu Varanasi<sup>1,2,\*</sup>

- <sup>1</sup> Bone-Muscle Research Center, College of Nursing and Health Innovation, University of Texas at Arlington, Arlington, TX 76010, USA
- <sup>2</sup> Department of Material Science and Engineering, University of Texas at Arlington, Arlington, TX 76010, USA
- <sup>3</sup> Department of Chemistry and Biochemistry, University of Texas at Arlington, Arlington, TX 76010, USA
- <sup>4</sup> Center for Engineering Complex Tissues, Center for Excellence in Tissue Engineering, Rice University, Houston, TX 77005, USA
- <sup>5</sup> Department of Oral and Maxillofacial Surgery, University of Texas Health Science Center at Houston, Houston, TX 77054, USA
- \* Correspondence: kamal.awad@uta.edu (K.A.); venu.varanasi@uta.edu (V.V.); Tel.: +817-272-1743 (V.V.)
- † These authors contributed equally to this work.

**Abstract:** Healing in compromised and complicated bone defects is often prolonged and delayed due to the lack of bioactivity of the fixation device, secondary infections, and associated oxidative stress. Here, we propose amorphous silicon oxynitride (SiON<sub>x</sub>) as a coating for the fixation devices to improve both bioactivity and bacteriostatic activity and reduce oxidative stress. We aimed to study the effect of increasing the N/O ratio in the SiON<sub>x</sub> to fine-tune the cellular activity and the antioxidant effect via the NRF2 pathway under oxidative stress conditions. The *in vitro* studies involved using human mesenchymal stem cells (MSCs) to examine the effect of SiON<sub>x</sub> coatings on osteogenesis with and without toxic oxidative stress. Additionally, bacterial growth on SiON<sub>x</sub> surfaces was studied using methicillin-resistant *Staphylococcus aureus* (MRSA) colonies. NRF2 siRNA transfection was performed on the hMSCs (NRF2-KD) to study the antioxidant response to silicon ions. The SiON<sub>x</sub> implant surfaces showed a >4-fold decrease in bacterial growth vs. bare titanium as a control. Increasing the N/O ratio in the SiON<sub>x</sub> implants increased the alkaline phosphatase activity >1.5 times, and the other osteogenic markers (osteocalcin, RUNX2, and Osterix) were increased >2-fold under normal conditions. Increasing the N/O ratio in SiON<sub>x</sub> enhanced the protective effects and improved cell viability against toxic oxidative stress conditions. There was a significant increase in osteocalcin activity compared to the uncoated group, along with increased antioxidant activity under oxidative stress conditions. In NRF2-KD cells, there was a stunted effect on the upregulation of antioxidant markers by silicon ions, indicating a role for NRF2. In conclusion, the SiON<sub>x</sub> coatings studied here displayed bacteriostatic properties. These materials promoted osteogenic markers under toxic oxidative stress conditions while also enhancing antioxidant NRF2 activity. These results indicate the potential of SiON<sub>x</sub> coatings to induce *in vivo* bone regeneration in a challenging oxidative stress environment.

**Keywords:** silicon oxynitride; reactive oxygen species; plasma-enhanced chemical vapor deposition; antioxidant activity; osteogenic differentiation



**Citation:** Ahuja, N.; Awad, K.; Yang, S.; Dong, H.; Mikos, A.; Aswath, P.; Young, S.; Brotto, M.; Varanasi, V. SiON<sub>x</sub> Coating Regulates Mesenchymal Stem Cell Antioxidant Capacity via Nuclear Erythroid Factor 2 Activity under Toxic Oxidative Stress Conditions. *Antioxidants* **2024**, *13*, 189. <https://doi.org/10.3390/antiox13020189>

Academic Editor: Maria-Jose Alcaraz

Received: 1 December 2023

Revised: 9 January 2024

Accepted: 11 January 2024

Published: 1 February 2024



**Copyright:** © 2024 by the authors. Licensee MDPI, Basel, Switzerland. This article is an open access article distributed under the terms and conditions of the Creative Commons Attribution (CC BY) license (<https://creativecommons.org/licenses/by/4.0/>).

## 1. Introduction

High-energy traumatic bone injuries, infections requiring surgical debridement, and large tumor resections result in large bone defects that are often associated with compromised wound healing resulting from deficient vascularization, hypoxia, wound contamination, or chemoradiotherapy [1,2]. These factors further complicate the defect healing

process due to the accumulation of reactive oxygen species (ROS) and prolonged inflammation which may not be eliminated by the protective antioxidant mechanisms in the body [3–5]. This accumulation of excessive toxic radicals of ROS leads to oxidative stress which increases osteoclastic activity and disrupts the bone remodeling process [4,6]. Prolonged oxidative stress causes damage to the nuclear acids and proteins, causing irreparable cellular injury and restricting cell viability, growth, and proliferation. Exogenous or dietary antioxidants have been shown to reduce ROS levels and increase osteocalcin activity via increased antioxidant activity [3,7–9] (e.g., nuclear erythroid factor 2 (NRF2), superoxide dismutase (SOD1), and glutathione peroxidase (GPX)). Yet, these exogenous approaches are unable to overcome the challenges of spontaneous healing and completely regenerating large bone defects [10]. Further, an alternative approach of using the local delivery of small-molecule antioxidant agents in biomaterials can intrinsically induce rapid cell recruitment, maintain viability, and provide the surface needed to support healing. Thus, antioxidants play a central role in lowering ROS levels while inducing angiogenesis and osteogenesis.

It has been established in pertinent literature that NRF2 is a key transcriptional factor responsible for activating an antioxidant response reaction against oxidative stresses [11,12]. NRF2 can be promoted during a traumatic injury or fracture, which induces a defense mechanism towards oxidative stress and regulates the bone healing rate [13,14]. NRF2 plays a vital role in promoting bone and vascular healing by enhancing cell viability and inducing migration, endothelial cell angiogenesis, and mesenchymal stem cell osteogenesis [15,16]. NRF2 also acts as a master antioxidant promoter that reduces ROS levels to promote healing. NRF2 is activated by two key mechanisms: (1) the phosphorylation of cell surface glycogen synthase kinase (p-GSK3-beta), which activates the promoter regions of the NRF2 gene, and (2) the presence of electrophilic compounds, such as sulforaphane, which can indirectly affect Kelch-like ECH-associated protein (Keap1)–NRF2 nuclear binding through the modification of cysteine residues on the Keap1 surface which subsequently affect NRF2 activity [11,14,16,17].

Current treatment options for large and compromised bone defects involve the use of fixative implants such as titanium implants for functional reconstruction. However, these materials are not bioactive and lack antioxidant properties [18,19], and their use sometimes leads to microbial biofilm formation, causing infection [20]. The consequent poor osteointegration, implant loosening, and failure further compromise the healing process [21,22]. Various coating materials are being actively studied to overcome these disadvantages [23–27]. Yet, failure due to thermal expansion mismatch [28–31], poor coating quality owing to high temperatures (>700 °C), reduced bioactivity [32,33], and reduction in osteogenic activity [34], resulting in immature bone healing and fibrous tissue attachment [35] and poor long-term stability [36], are problems which still need to be addressed. New biomaterials or coatings on already existing biomaterials/fixative materials that can precisely enhance the wound healing environment are thus urgently needed for volumetric bone repair.

Our previous studies have shown that SiON<sub>x</sub> and silicon oxynitrophosphide (SiONP<sub>x</sub>) coatings induce antioxidant activity that reduces ROS levels and inflammation, resulting in early bone tissue regeneration [37–41]. Similarly, silica (SiO<sub>2</sub>)-based nanoparticles/surface modifications have been widely studied for their antibacterial properties [42]. SiON<sub>x</sub> films formed by plasma-enhanced chemical vapor deposition (PECVD) have been applied to a myriad of substrates, including Si wafers [37,40], metal devices such as titanium devices [43], and even ceramics and polymers [44]. We have conducted such studies and have found that irrespective of the substrate type, the coatings always maintain an amorphous structure, and their binding chemistry forms a covalent/ionic bond with the substrate, as measured by X-ray diffraction, X-ray absorption near-edge structure (XANES) analysis, and electron microscopy analysis in microstructure and morphology studies [37–41,43,45,46]. SiON<sub>x</sub> is an amorphous material with varying levels of tetrahedral and trigonal chemical bond structure depending on the N/O ratio within the films [41]. This ratio is controlled by the material formation from source gases NH<sub>3</sub> and N<sub>2</sub>O under a reductive ionized

gas environment [41]. This approach is advantageous as the coating thickness, atomic ratio, and interfacial formation on a biomedical device can be precisely controlled [32,43]. Further, these materials can be fabricated at relatively low temperatures (<400 °C), due to which the thermal expansion mismatch between the implant substrate and the coating layers is markedly reduced. In addition, the film can be formed relatively quickly (within 1 h), simplifying the “made-to-order” or “patient defect tailored” manufacturing process. These bespoke SiON<sub>x</sub> nanolayered coatings on biomedical devices will lead to the targeted delivery of the required antibacterial and antioxidant effects to the defect/injury site.

Their application in our previous studies led to a reduction in the lipid peroxidation on the SiON<sub>x</sub>-coated implants along with an increase in the angiogenic activity [37]. The silicon oxynitride chemical structure contains a range of tetrahedral bonds with a low N/O ratio and trigonal bonds with a high N/O ratio. We previously demonstrated that the random bonding model (RBM) is valid for a low N/O ratio, whereas the random mixture model (RMM) is applicable for a high N/O ratio. We also showed that increasing the N/O ratio lowers the energy required for 2p to 3d electron transitions. The presence of 3d electron orbits is needed to stimulate antioxidant activity, which is spin-orbit-restricted and only becomes activated by transition metals with readily available 3d electrons (Zn, Cu, Mn, Fe). More fundamentally, an increase in the N/O ratio changes the partial charge and the surface dipole that affects how the surface will share electrons with attached cellular membranes in which biomolecules depend on the energy state of these surface electrons.

Hence, we aim to study the SiON<sub>x</sub> surface and the Si ion release effects on bacterial growth as well as MSC proliferation and differentiation *in vitro* with and without oxidative stress conditions to understand the underlying molecular mechanism. To achieve this objective, we use increasing nitrogen-to-oxygen ratio (N/O) in the Si–O–N composition as the independent variable. In this context, the N/O ratio essentially describes the solid-state substitution of O for N as it is added into the material and is dictated by the NH<sub>3</sub>/N<sub>2</sub>O gas flow in PECVD. The N/O ratio affects the local surface dipole that plays a role in the oxidative state (or valence state) of the surface. Subsequently, cells exposed to these surfaces with differing oxidative states can exhibit differences in viability, proliferation, and differentiation due to the ability of the surface to potentially affect how the cell interacts with its local environment. This effect can also be observed with biomaterials tested with osteogenic progenitors that can induce marker activity, such as alkaline phosphatase, as early as 1–7 days after exposure [47]. Thus, a detailed examination of these markers is needed to ascertain the full effect of the impact of these biomaterials.

Here, we study the effect of increasing nitrogen (N) content in SiON<sub>x</sub> surface coatings on the bacteriostatic effect, antioxidant activity, ROS, and osteogenesis. Finding the effective N/O ratio in a SiON<sub>x</sub> coating will enable the development of engineered coatings for fixative implantable materials with specific surface chemistry capable of triggering beneficial biological activity for faster bone healing. In the present study, attention is given to antioxidant activity maximization and thus enhancement in oxidative stress reduction. We propose that SiON<sub>x</sub> induces antioxidant activity and reduces oxidative stresses through the NRF2 pathway, and thus, we aim to uncover the role of the NRF2 signaling pathway in the SiON<sub>x</sub> antioxidant activity.

## 2. Materials and Methods

### 2.1. Fabrication of the Coatings

SiON<sub>x</sub> and SiONP<sub>x</sub> thin film coatings were fabricated using the PECVD technique according to our previously published methods [37,39–41,43,45,48]. Briefly, the surface was prepared for the coatings by applying standard cleaning procedures based on the piranha solution (3:1 mixture of sulfuric acid (H<sub>2</sub>SO<sub>4</sub>, 96%) and hydrogen peroxide (H<sub>2</sub>O<sub>2</sub>, 30%)) for 10 min and was subsequently rinsed in deionized (DI) water for 1 min. Then, a TRION ORION II PECVD/LPECVD system (Trion Technology, Clearwater, FL, USA) was used to deposit a 1000 nm thin film coating of SiON<sub>x</sub> or SiONP<sub>x</sub> on a silicon wafer. Increasing the N<sub>2</sub>O gas flow rate increases the oxygen incorporation in the coatings relative to the

nitrogen content. Thus, five different SiON<sub>x</sub> chemistries were fabricated based on changing the N<sub>2</sub>O flow rate. The refractive index (*n*) of the deposited coatings was measured and was used to distinguish the coatings in this study. Refractive index values ranged from *n* = 2 for N<sub>2</sub>O = 0 standard centimeters cubed per minute (sccm) to *n* = 1.45 for N<sub>2</sub>O = 160 sccm. The study groups were as follows: (1) positive control (tissue culture plate surface), (2) *n* = 1.45, (3) *n* = 1.57, (4) *n* = 1.65, (5) *n* = 1.82, and (6) *n* = 2. The same methods were used for obtaining SiONP<sub>x</sub>, with the exception of phosphine gas (PH<sub>3</sub>) as a phosphorus source, as shown in Table 1. The composition of the coatings, the exact flow rate, and the refractive index of each coating are provided in Table 1.

**Table 1.** Gas flow rates, deposition rate, and refractive index for SiON<sub>x</sub> or SiONP<sub>x</sub> layers deposited by PECVD.

Sample	Coating	Gas Flow Rate (sccm)				Deposition Rate (nm/min)	Refractive Index ( <i>n</i> )
		15% SiH <sub>4</sub> /Ar	N <sub>2</sub> O	N <sub>2</sub>	NH <sub>3</sub>		
1	SiON <sub>x</sub>	24	160	225	50	62.5	1.45
2		24	155	225	50	59.5	1.57
3		24	16	225	50	44.5	1.65
4		24	3	225	50	41.0	1.82
5		24	0	225	50	36.5	2.0
6	SiONP <sub>x</sub>	15%SiH <sub>4</sub> /2%PH <sub>3</sub> /Ar	N <sub>2</sub> O	N <sub>2</sub>	NH <sub>3</sub>	Deposition Rate	Refractive index ( <i>n</i> )
		24	16	225	50	38.5	1.68

## 2.2. In Vitro Studies

Human bone marrow mesenchymal stem cells (MSCs) were obtained from Lonza (Lonza Walkersville Inc., Walkersville, MD, USA). All cells were authenticated, performance assayed, and tested negative for mycoplasma, according to the provider. MSCs (passages 2–4) were grown according to the Lonza protocol in MSCGM BulletKit™ (Lonza, PT-3238 and PT-4105) specific growth medium at 37 °C and 5% CO<sub>2</sub> in a completely humidified incubator. For studying the effect of increasing nitrogen concentration in the coatings, the following groups (*n* = 4) were used for all in vitro studies: I—tissue culture plate (TCP); II—SiON<sub>x</sub> *n* = 1.45; III—SiON<sub>x</sub> *n* = 1.57; IV—SiON<sub>x</sub> *n* = 1.65; V—SiON<sub>x</sub> *n* = 1.82; and VI—SiON<sub>x</sub> *n* = 2. Cells (5000–6000 cells/cm<sup>2</sup>) were seeded on TCP as control and SiON<sub>x</sub> with different refractive indices and were allowed to grow for 7 days. All samples were cleaned using 100% ethanol followed by dry heat sterilization prior to each experiment [49].

In vitro cytotoxicity studies were performed according to our previously reported protocols [43,45]. Cytotoxicity and cell adhesion, viability, and proliferation were studied at 1, 4, and 7 days. The MTS-CellTiter<sup>96</sup>® Aqueous One Solution Cell Proliferation Assay (Promega, Madison, WI, USA) was used for the quantitative analysis of cell growth and proliferation. The LIVE/DEAD™ Viability/Cytotoxicity Stain Kit (Thermo Fischer Scientific Inc., Waltham, MA, USA) was utilized for the qualitative analysis of cell adhesion and viability on the tested surfaces. Both assays were performed according to the manufacturer's instructions and our previously published protocols [37,45]. The colorimetric absorbance of the MTS assay was determined using a microplate reader (SpectraMax® i3, Molecular Devices, San Jose, CA, USA) at 490 nm. Normal and oxidative cell culture media without cells were used to account for any background that is subtracted from all MTS absorbance results. Live/dead fluorescence images were then taken using a DMi8 inverted Leica microscope (Leica Microsystems Inc., Deerfield, IL, USA), with green fluorescent calcein-AM for live cells and red fluorescent ethidium homodimer-1 for dead cells.

To induce osteogenic differentiation of the MSCs, hMSC differentiation BulletKit™—osteogenic was acquired from Lonza, PT-3002; it contains osteogenic differentiation basal medium and hMSC osteogenic SingleQuots™. All groups described above were used for all differentiation studies, including TCP as the control and SiON<sub>x</sub>

with different refractive indices. Differentiation studies were conducted for 7 days, with media collected for analysis on days 1, 4, and 7.

To study the effect of SiON<sub>x</sub> on the osteogenic differentiation of MSCs, an Alkaline Phosphatase (ALP) Kit (Colorimetric) (Abcam, Waltham, MA, USA) was used to quantify the ALP activity in the collected media for differentiated MSCs after 1, 4 and 7 days.

Human umbilical vein endothelial cells (HUVECs) (passages 2 to 4), endothelial cell growth medium 2 (EGM-2) (used for cell growth and subculture), and endothelial cell basal media 2 (EBM-2) (used for the proliferation and differentiation experiments) were acquired from Lonza®. These cells were seeded at a concentration similar to that of the MSCs and were allowed to culture for several days prior to lysis.

After 7 days of differentiation, RNA was collected from the differentiated MSCs, purified using the miRNAeasy MINI KIT from QIAGEN®, and converted to cDNA using the Goscript™ Reverse transcriptase kit from Promega Corporation. Reverse transcription polymerase chain reaction (RT-PCR) was performed using the TaqMan® Gene Expression Assay with the standard protocol adjusted for 40 cycles. The obtained results were expressed relative to the housekeeping gene GAPDH and compared to the control (TCP), and the delta Ct method was used for calculations. Osteogenic markers RUNX2 (Runt-related transcription factor-2), BGLAP (osteocalcin, also OCN), ALP (alkaline phosphatase), and SP7 (Osterix) were assessed.

For OCN detection by immunohistochemistry, after 7 days of differentiation, the cell culture well plates were washed with PBS, fixed, and blocked with 10% goat serum. After blocking, the primary antibodies (Rabbit polyclonal OCN 1:500) were placed on the slides and incubated overnight at 40 °C. Then, Alexa Dye 594 Goat anti-Rabbit secondary antibodies in 1:200 dilution were introduced, and the sample was incubated for 1–2 h, washed twice with PBS, stained with DAPI for 15–20 min at room temperature, and evaluated under a DMi8 inverted Leica microscope (Leica Microsystems Inc., IL, USA).

Hydrogen peroxide (H<sub>2</sub>O<sub>2</sub>) was used to induce oxidative stress in the cells. H<sub>2</sub>O<sub>2</sub> has been used in various in vitro studies as a major product of oxidative stress, produced by swift conversion from superoxide. A preliminary study was conducted using different H<sub>2</sub>O<sub>2</sub> concentrations (0–1 mM) to determine the optimal H<sub>2</sub>O<sub>2</sub> amount for mimicking an oxidative stress environment deleterious for the cells. A 30% *w/w* of H<sub>2</sub>O<sub>2</sub> with stabilizer stock solution was acquired from Sigma-Aldrich. Based on the obtained findings, we determined 0.2 mM as the H<sub>2</sub>O<sub>2</sub> concentration that is deleterious for the MSCs.

All cell culture studies stated above—including the cell viability and proliferation (MTS and live/dead assay) along with differentiation studies (ALP assay, PCR, IHC)—were repeated under oxidative stress conditions by introducing 0.2 mM of H<sub>2</sub>O<sub>2</sub> to the cell culture environment. Additionally, antioxidant markers—nuclear factor erythroid 2-related factor 2 (NRF2) and Keap1—were utilized for the oxidative stress study.

We acquired human NRF2 siRNA from Santa Cruz Biotechnology, Inc. (SC-37030), Dallas, TX, USA, to knock down NRF2 (NRF2-KD) in the MSCs. We followed the manufacturer's protocol to perform NRF2 siRNA transfection. The MSCs were seeded in a 6-well plate as described above and were incubated until 60–80% confluence was achieved. We prepared two transfection solutions (A and B). For obtaining Solution A, 6 µL of siRNA duplex was added to 100 µL of siRNA Transfection Medium (sc-36868) for each transfection, and for Solution B, 6 µL of siRNA Transfection Reagent (sc-29528) was added to 100 µL of siRNA Transfection Medium (sc-36868) for each transfection. The two solutions were mixed gently, and the resulting mixture was incubated for 15–30 min at room temperature before adding 0.8 mL of siRNA Transfection Medium. Next, the seeded cells were washed twice and then incubated at 37 °C with the siRNA Transfection Reagent for 6–7 h. After transfection, the reagent was removed and replaced with normal growth medium. The cells were allowed to grow for 4 days prior to the PCR analysis. We also performed an internal control for the siRNA transfection which included a scrambled sequence that would not lead to the specific degradation of any known cellular mRNA.

As staphylococci account for up to two-thirds of all pathogens isolated from orthopedic implant infections, methicillin-resistant *Staphylococcus aureus* (MRSA) bacterial assays were conducted to study the bacterial growth on the implant surfaces. When using MRSA, the ASTM and ISO standards for In Vitro Test Methods for Antimicrobial Coatings on Medical Devices were followed [50]. These bacteria form a biofilm on the surface of a foreign device such as a metallic implant, making infection eradication without the surgical removal of the device impossible. A biofilm is a community of sessile bacteria encased in an extracellular matrix comprising water, microbial cells, nutrients, polysaccharides, DNA, and proteins. The biofilm provides a protective matrix around the encased bacteria and is highly resistant to host immune defenses and antimicrobials [51]. Thus, MRSA was used to evaluate the bacteriostatic effect of the studied coatings as potential surface coatings for biomedical metallic implants. For each experiment, a single colony from the inoculation plate was used with Mueller Hinton Broth (MHB) as the medium. A total of  $10^5$  colony-forming units/mL (CFU/mL) was seeded onto the material surface with an inoculation loop, and the samples were dried to remove all liquid and then incubated at 37 °C for 12, 24, or 48 h. A live/dead bacteria assay kit (LIVE/DEAD BacLight Bacterial Viability Kit, Thermo Fischer Scientific Inc., Waltham, MA, USA) was used to stain the bacteria on the surfaces for 15 min at room temperature, after which the samples were washed with PBS and imaged under an EVOS M5000 Imaging System. ImageJ software (NIH, version 1.53k) was used to further analyze the results.

### 2.3. Statistical Methods

The results are presented in box plots showing the mean, standard deviation, and significance levels. One-way ANOVA (Tukey's pairwise comparison) was conducted to compare the means of more than two groups at a significance level of  $p < 0.05$ , and image analysis was performed in ImageJ. OriginPro 2017, Past3, and Microsoft Excel 2016 Software were used for graphics and calculations.

## 3. Results

As mentioned above, we have several publications on the PECVD  $\text{SiON}_x$ - and  $\text{SiONP}_x$ -based coatings examined here, and we have established their amorphous nature with unique surface characteristics. Therefore, the chemical composition, structure, and surface morphology of the deposited coatings were characterized to ensure full compliance with our published data (see reference [41] for a comprehensive characterization of these coatings). The coatings were characterized using XRD, XANES, FT-IR, XPS, NRA-RBS, HR-SEM with EDX, and HR-TEM [37–39,41,43,48]. Thus, the work presented here focuses on the bacteriostatic effect and the molecular mechanism behind the antioxidant activity of these coatings.

### 3.1. Bacteriostatic Effect

We studied the bacterial growth and MRSA adherence on the various  $\text{SiON}_x$  chemistries compared to the titanium surface (positive control). The quantitative analysis of the live MRSA bacteria on  $\text{SiON}_x$ -coated surfaces compared to titanium after 12, 24, and 48 h (calculated by ImageJ software) is shown in Figure 1. A significant decrease in cell viability and proliferation is evident in all  $\text{SiON}_x$ -coated samples, as indicated by a decrease in green staining (live bacteria) and an increase in red staining (dead bacteria) at 48 h (Figure 2). (Supplemental Figures S1.1 and S1.2 represent bacterial live/dead stains at 12 and 24 h, respectively.) A significant decrease in bacterial counts at 12 h was noted on the high-N/O-ratio  $\text{SiON}_x$  ( $n = 2.0$ ) surface, which exhibited the lowest bacterial counts amongst all  $\text{SiON}_x$  groups after 24 and 48 h. This finding is indicative of a bacteriostatic effect on the  $\text{SiON}_x$ -coated surfaces inhibiting bacterial growth and proliferation compared to titanium.

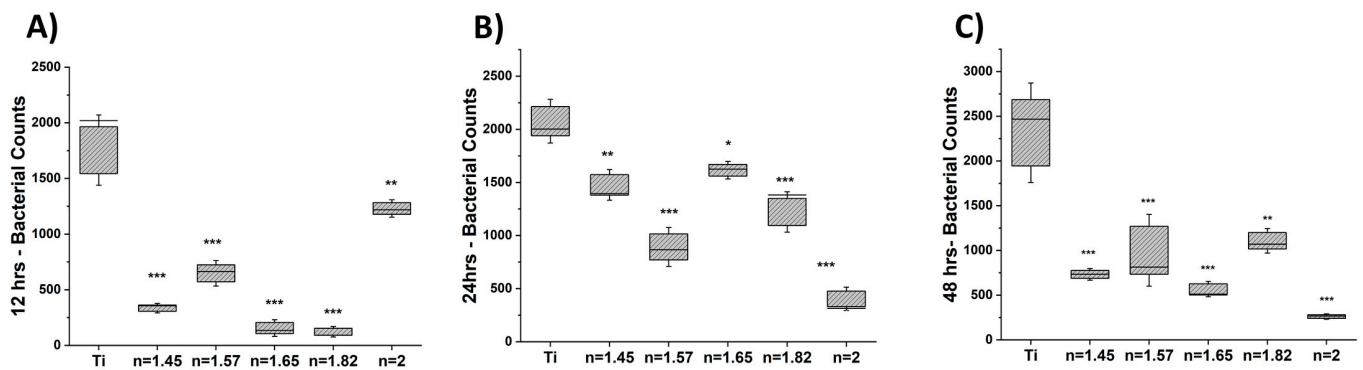


**Figure 1.** Bacteriostatic effect of SiON<sub>x</sub> versus Ti. All SiON<sub>x</sub> samples presented a significant decrease in the total number of bacteria at all time points: (A) 12 h, (B) 24 h, and (C) 48 h. At 12 h, the lowest bacterial counts were noted for SiON<sub>x</sub> ( $n = 1.82$ ), while the bacterial counts on SiON<sub>x</sub> ( $n = 2.0$ ) significantly decreased at 24 and 48 h. \*  $p < 0.05$ , \*\*  $p < 0.01$ , and \*\*\*  $p < 0.001$  present the significance compared to Ti as a control.

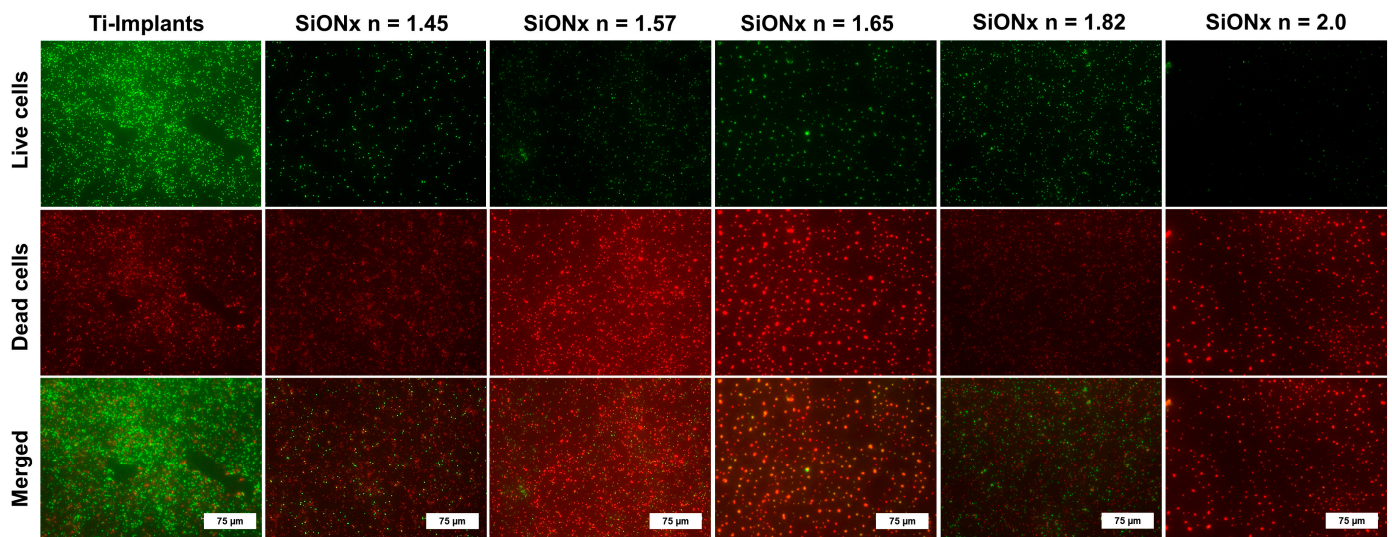


**Figure 2.** Bacteriostatic effect of SiON<sub>x</sub> coatings versus Ti-based implants. Fluorescence images show the live (green) and dead (red) bacteria on different SiON<sub>x</sub> surfaces compared to Ti-based implants after 48 h.

### 3.2. Cell Viability and Proliferation under Normal Conditions

We studied the MSC viability, growth, and proliferation on various SiON<sub>x</sub> chemistries to evaluate the effect of increasing the nitrogen content relative to oxygen while keeping the silicon content in the coatings fixed. We performed an MTT assay for quantitative analysis along with qualitative live/dead fluorescence analysis (Calcein AM and Ethidium homodimer) after 1, 4, and 7 days of seeding on the various SiON<sub>x</sub> surfaces. As can be seen from Figure 3, there are no significant differences among the groups or between groups and the positive control (TCP surface) on days 1 and 4 of cell proliferation under normal conditions, suggesting normal growth. However, after 7 days, cellular proliferation decreases as the N/O ratio increases, which can be attributed to MSC detachment on the un-patterned base silicon wafer surface.

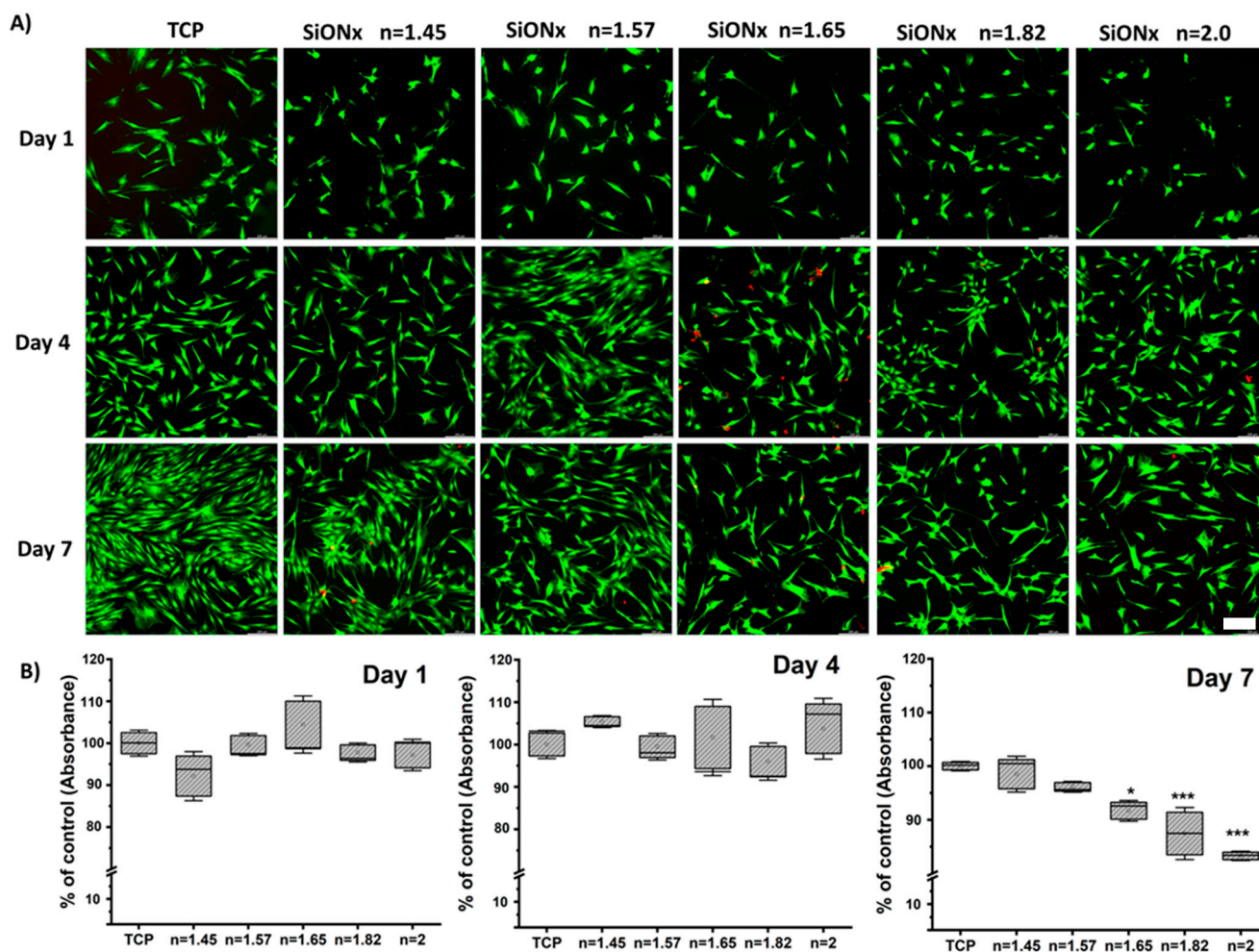


**Figure 3.** Cell viability and proliferation assay evaluated by (A) fluorescent live (Calcein AM) (green stain) and dead (Ethidium homodimer) (red stain) staining along with quantitative evaluation by (B) MTS assay after 1, 4, and 7 days of seeding on the various SiON<sub>x</sub> surface chemistries. \*  $p < 0.05$  and \*\*\*  $p < 0.001$  present the significance compared to the normal TCP as a control. Scale bar = 200  $\mu\text{m}$ .

### 3.3. Osteogenic Differentiation with Increasing N/O Ratio in SiON<sub>x</sub> Surfaces

We studied the alkaline phosphatase (ALP) activity on various SiON<sub>x</sub> chemistries using the Alkaline Phosphatase Assay Kit (Figure 4) and the cell culture supernatant of the seeded MSCs undergoing osteogenic differentiation at 1, 4, and 7 days. No significant differences in the ALP activity in SiON<sub>x</sub>  $n = 1.82$  and  $n = 2$  were noted when compared to the control (TCP) on days 1 and 4. On day 7, there was significantly less ALP activity in the media supernatant of the SiON<sub>x</sub> samples as compared to the control, which was attributed to the decrease in the cellular numbers as noted above. However, there was a significant increase in the ALP activity as the SiON<sub>x</sub> nitrogen content increased relative to oxygen on day 7 (the SiON<sub>x</sub>  $n = 2$  group exhibited the highest activity level).

Gene expression analysis (rt-PCR) (Figure 5) reveals an upregulation of osteogenic markers (osteocalcin, ALPL, and Osterix) with an increase in the N/O ratio in the SiON<sub>x</sub> as compared to the control. There is  $>2\text{--}3\times$  upregulation of osteogenic markers in SiON<sub>x</sub>  $n = 1.82$  and  $n = 2$  as compared to the control and the other SiON<sub>x</sub> chemistries. Figure 6 depicts a similar upregulation of the antioxidant markers (SOD1, NRF2, and GPX1) with the increase in the N/O ratio in the SiON<sub>x</sub> as compared to the control. Although there is a 2-fold upregulation in the antioxidant activity, the values are not significantly different from the baseline (with the exception of GPX1 for SiON<sub>x</sub>  $n = 2$ ).

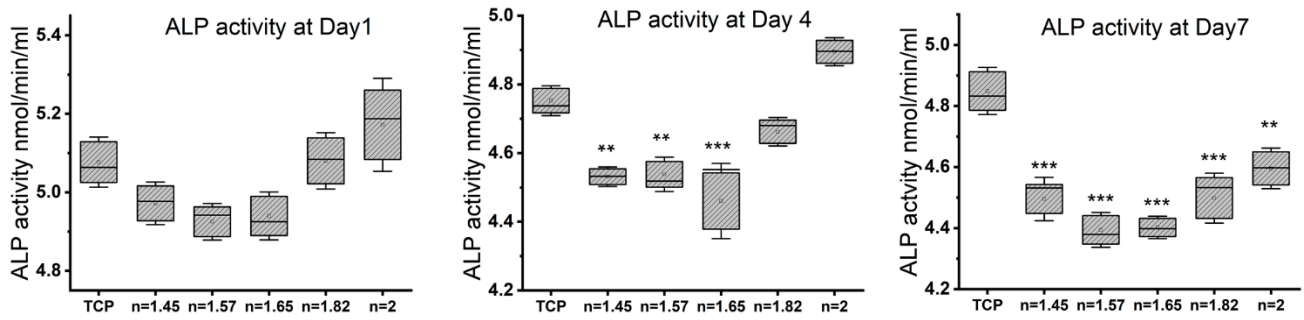


**Figure 4.** Alkaline phosphatase assay on days 1, 4, and 7 of osteogenic differentiation in MSCs on different SiON<sub>x</sub> chemistries. The ALP activity in SiON<sub>x</sub> *n* = 1.82 and *n* = 2 is not significantly different when compared to the control on days 1 and 4. \*\* *p* < 0.01 and \*\*\* *p* < 0.001 present the significance compared to the normal TCP as a control.

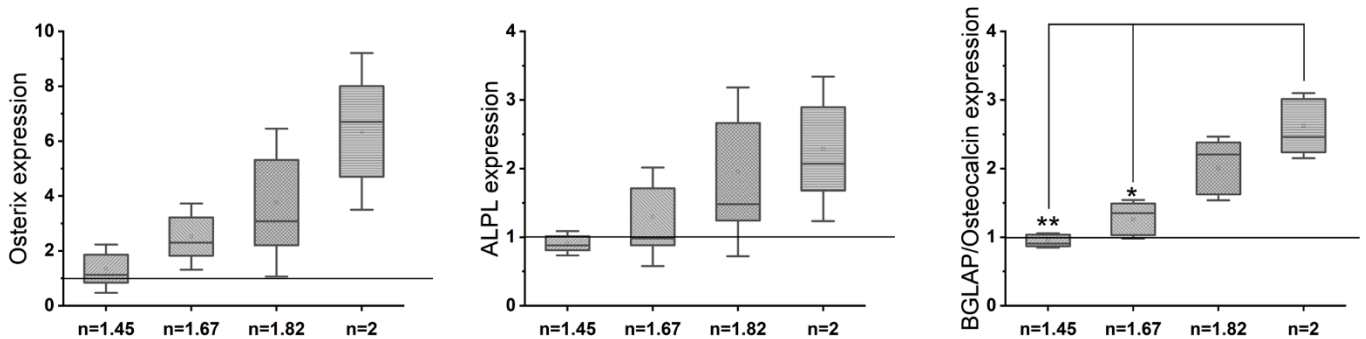


**Figure 5.** Gene expression analysis (rt-PCR) shows an upregulation of osteogenic markers on SiON<sub>x</sub> as compared to the baseline control. The increase in the N/O ratio increases the osteogenic marker expression. \* *p* < 0.05 and \*\* *p* < 0.01 present the significance compared to the normal TCP as a control.

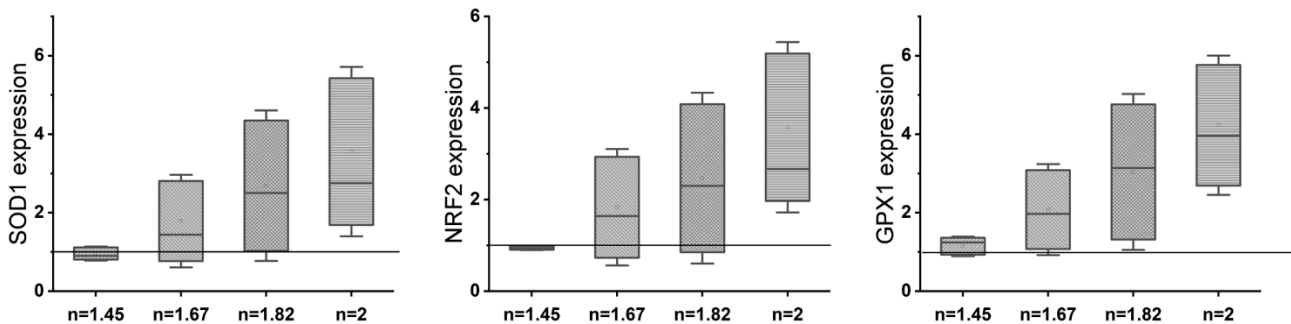


**Figure 6.** Gene expression analysis (rt-PCR) shows an upregulation of antioxidant markers in SiON<sub>x</sub> as compared to the baseline control. The increase in the N/O ratio increases the antioxidant marker expression.

### 3.4. Determining Minimal H<sub>2</sub>O<sub>2</sub> Concentration for Inducing Oxidative Stress in MSCs

Hydrogen peroxide has been used in extant studies to induce oxidative stresses in the cellular environment. To determine the minimal H<sub>2</sub>O<sub>2</sub> concentration that would have a deleterious effect on the MSC growth, we tested the cell viability (MTT and live/dead assay) after adding H<sub>2</sub>O<sub>2</sub> in various concentrations (0.2 mM, 0.4 mM, 0.6 mM, 0.8 mM, and 1 mM) to the culture media (0 mM served as the control). As shown in Figure 7, a significantly lower number of live cells (15–20% less) was present at 0.2 mM and 0.4 mM, while more than 60% reduction in cell survival was noted at 0.6 mM, and almost all cells died at higher concentrations. We removed the oxidative stress medium after 24 h and placed the surviving cells on the normal growth medium for 3 days. We observed that

even after the removal of the initial oxidative stress, there was a sustained insult on the cell survival. Hence, we chose 0.2 mM as our final concentration as there was a significant effect of the toxic oxidative stress environment and, on further growing the cells after the initial insult, the cell survival rate exceeded 60% (Supplemental Figure S2).

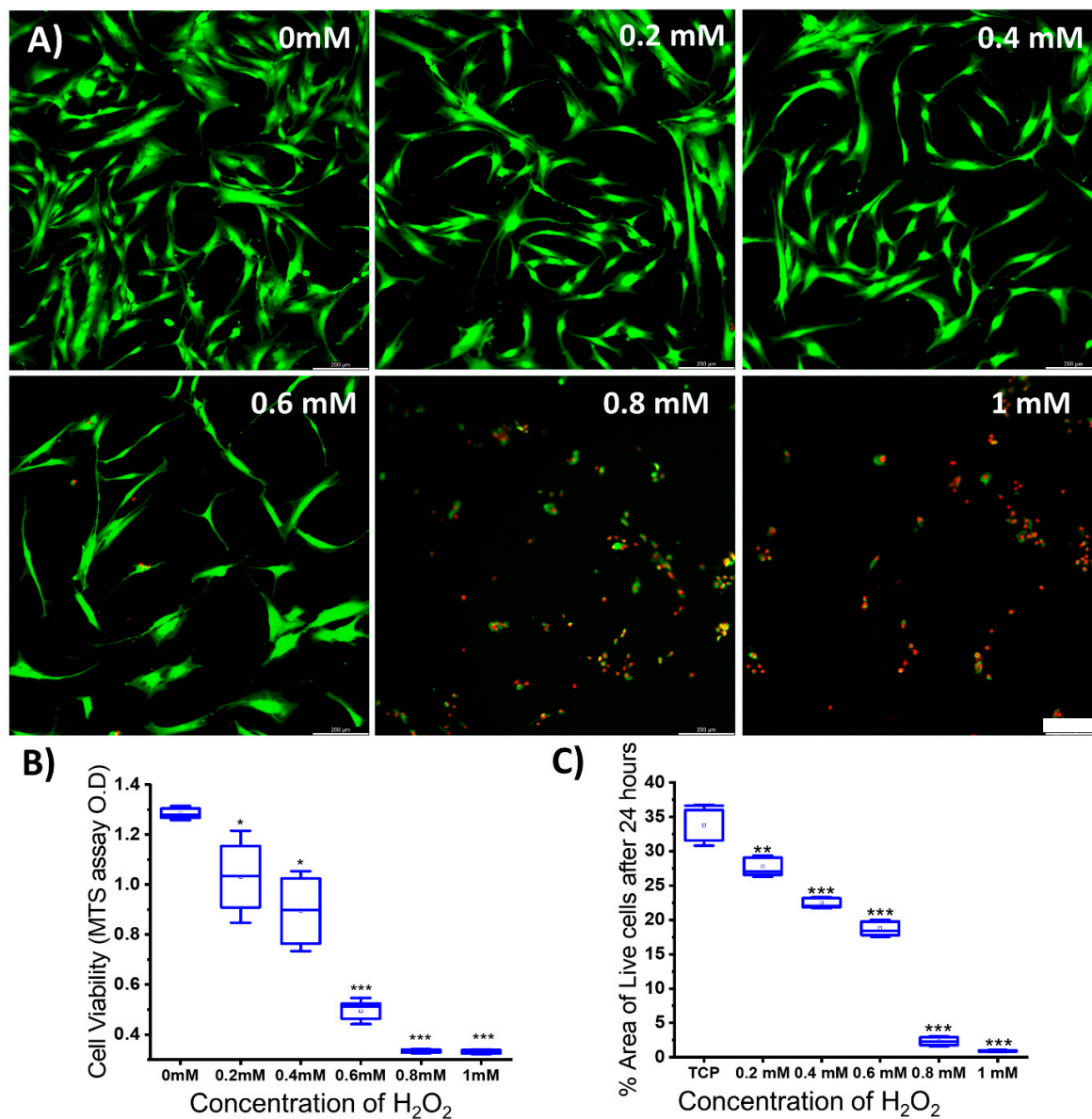


**Figure 7.** (A) Cell viability tested under various hydrogen peroxide concentrations; (B) MTS assay; (C) quantification of live cells using ImageJ software. \*  $p < 0.05$ , \*\*  $p < 0.01$ , and \*\*\*  $p < 0.001$  present the significance compared to the normal control of 0 mM H<sub>2</sub>O<sub>2</sub> or the TCP as a control. Scale bar = 200  $\mu$ m.

### 3.5. Effect of Increasing the Nitrogen Concentration in SiON<sub>x</sub> Chemistry on the Cell Proliferation and Differentiation under Oxidative Stress Conditions

We further analyzed the effect of cell viability and growth by MTS assay and live/dead staining on MSCs when seeded on the various SiON<sub>x</sub> chemistries under toxic oxidative conditions. Figure 8 shows that increasing the nitrogen content relative to oxygen (when silicon is kept constant) has a protective effect on the MSCs against the toxic oxidative stress, showing a 2-fold increase in the number of cells on  $n = 2$  as compared to  $n = 1.45$  and  $n = 1.57$  and showing a comparable number of cells to that recorded when no hydrogen peroxide was present in the environment. PCR analysis performed after differentiating the

MSCs in an osteogenic medium for 7 days after the initial exposure to the oxidative stress environment reveals an increase in the RUNX2 upregulation (Figure 9) in SiON<sub>x</sub>  $n = 1.82$  when compared to the baseline with oxidative stress as well as the other studied SiON<sub>x</sub> chemistries, while being comparable to the control with no oxidative stress. There is also a significant upregulation in ALPL and osteocalcin with SiON<sub>x</sub>  $n = 1.82$  compared to the baseline with/without oxidative stress as well as the other studied SiON<sub>x</sub> chemistries (Figure 9).

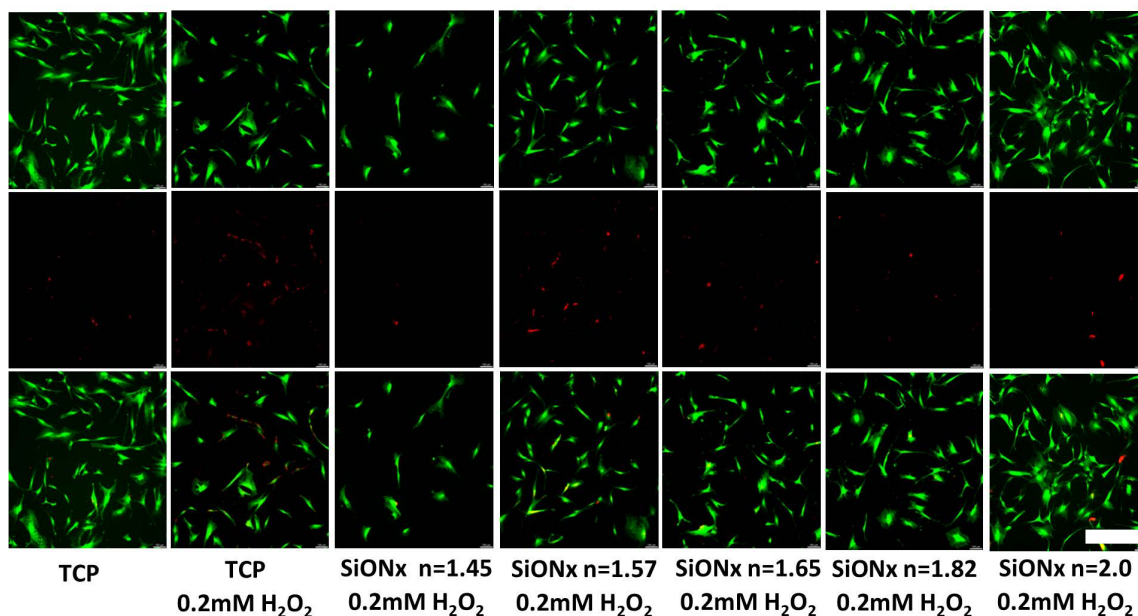


**Figure 8.** Cell proliferation on various SiON<sub>x</sub> chemistries under toxic oxidative stress. Green color (stained by Calcein AM) represents the live cells, and red color (stained by Ethidium homodimer) represents the dead cells. Scale bar = 200  $\mu$ m.

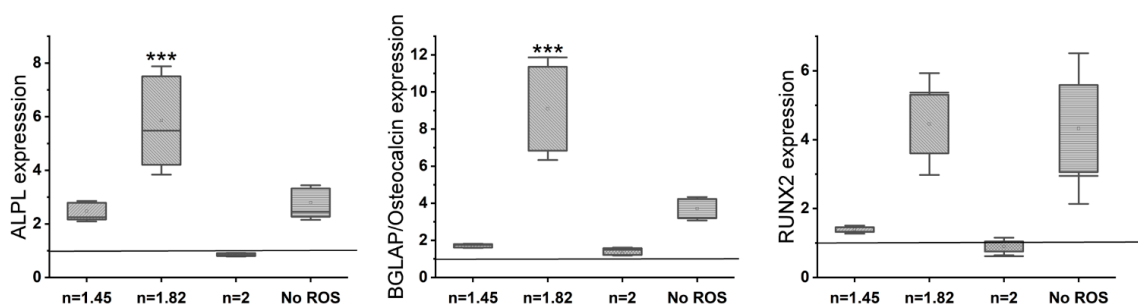


**Figure 9.** Gene expression analysis (rt-PCR) shows a significant upregulation of osteogenic markers in SiON<sub>x</sub>  $n = 1.82$  as compared to the baseline control in an oxidative stress environment. The osteogenic marker expression is not significantly different from the baseline with no oxidative stress involvement. \*\*\*  $p < 0.001$  presents the significance compared to the control.

Florescent microscopy also reveals significantly enhanced osteocalcin (OCN) activity (Figure 10) on the SiON<sub>x</sub> surface. Antioxidant markers (SOD1, NRF2, and GPX1) are significantly overexpressed in SiON<sub>x</sub>  $n = 1.82$ , which correlates to the overexpression of the oxidative markers in the same groups when compared to the baseline with oxidative stress and other SiON<sub>x</sub> chemistries, as well as the control group with no oxidative stress involved (Figure 11). Keap1 marker expression was increased compared to the control with no oxidative stress; however, no significant differences are observed within the groups. There was also an increase in the expression of antioxidant NRF2 activity (Figure 12) on the SiON<sub>x</sub> surface compared to the control.

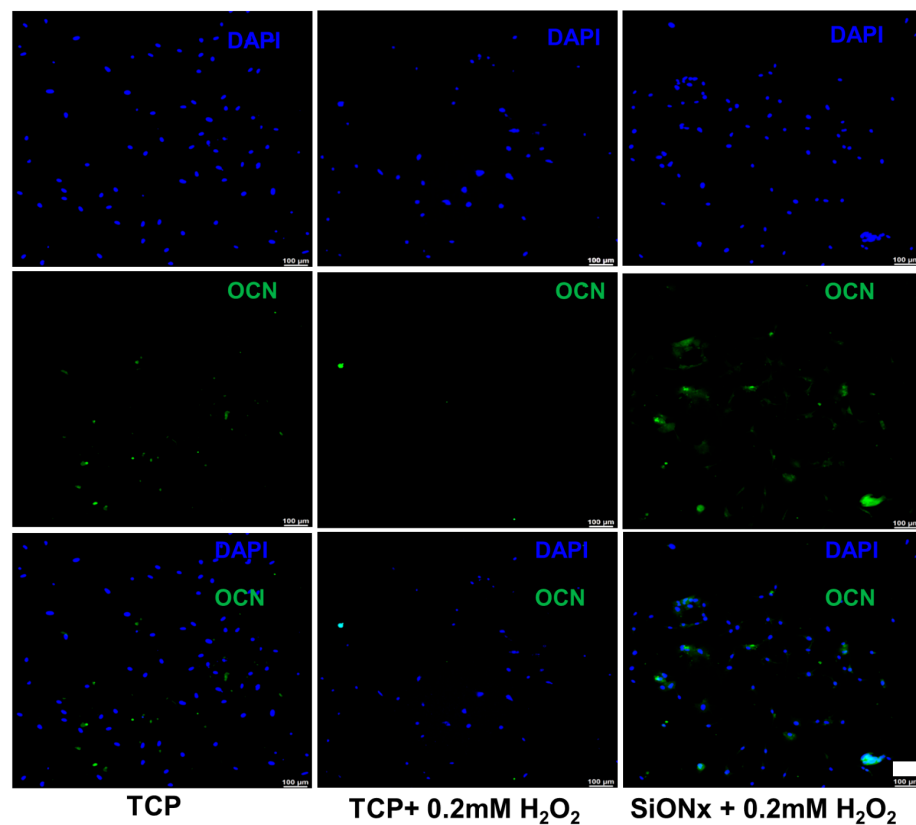


**Figure 10.** IHC staining representing DAPI (blue) and osteocalcin (green) on MSCs after 7 days of osteogenic differentiation. Overexpression of the osteogenic marker on the selected SiON<sub>x</sub> ( $n = 1.82$ ) surface vs. the control is evident. Scale bar = 100 µm.

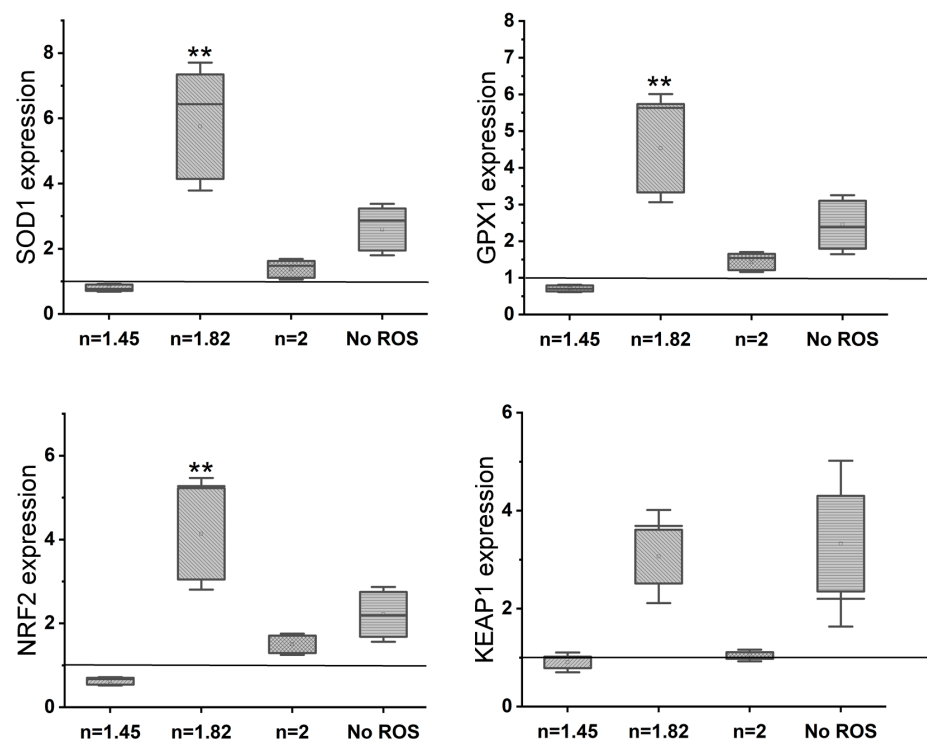


**Figure 11.** Gene expression analysis (rt-PCR) shows a significant upregulation of antioxidant markers in SiON<sub>x</sub>  $n = 1.82$  as compared to the baseline control in an oxidative stress environment. \*\*  $p < 0.01$  presents the significance compared to the baseline control (TCP).

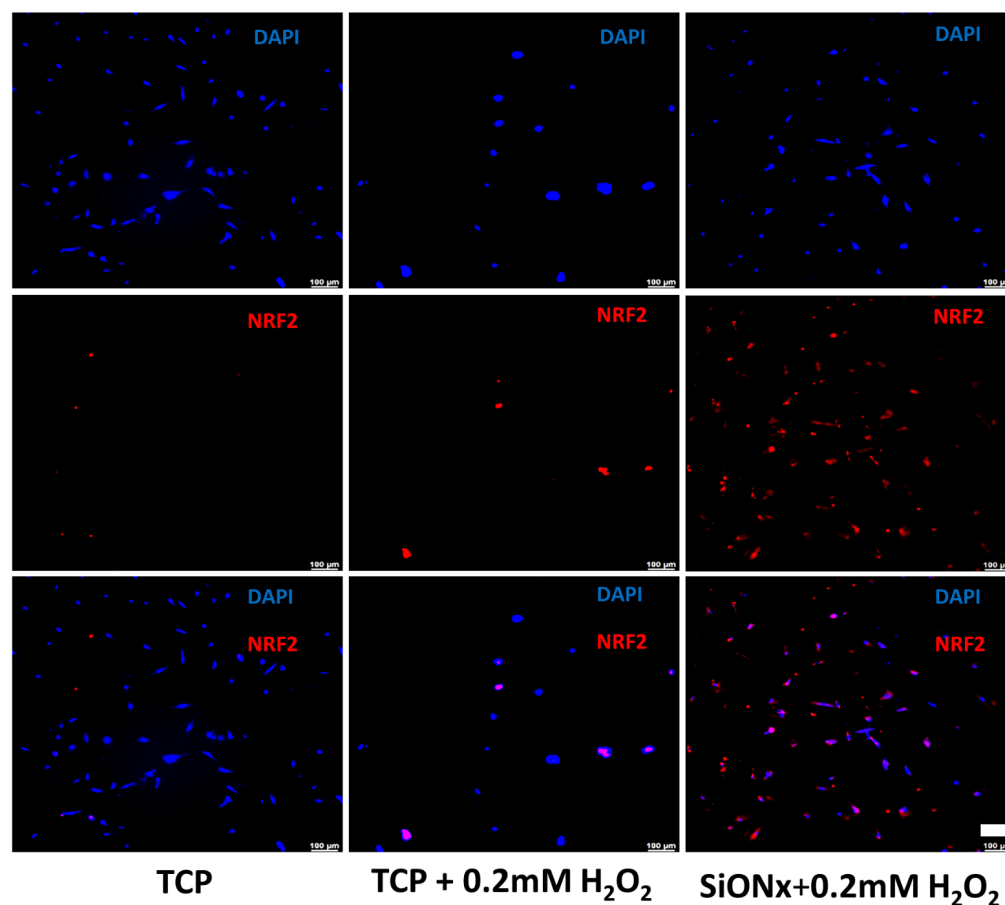


**Figure 12.** IHC staining representing DAPI (blue) and NRF2 (red) on MSCs after 7 days of osteogenic differentiation. There is a significant increase in the antioxidant NRF2 activity on the selected SiON<sub>x</sub> ( $n = 1.82$ ) surface when compared to the control. Scale bar = 100 µm.

We observed > 70% transfection with NRF2 siRNA after 6 h of incubation. Next, to study the effect of silicon on NRF2 and antioxidant activity, we grew the MSCs in normal growth media for 4 days post-transfection and added 0.5 mM of Si ions. RT-PCR analysis after NRF2 KD revealed that the NRF2 activity remained suppressed even after the addition of Si ions (Figure 13). Antioxidant expression indicates that, in the absence of transfection, there is a 2-fold increase in the SOD1 and GPX1 expression (Figure 13). A similar effect is observed in the control transfection group (scrambled sequence with no effect on mRNA), although when NRF2 is knocked down, there is no increase in the antioxidant expression compared to the baseline (Figure 13). There are no significant differences between the no-transfection group and the NRF2.

We conducted further testing to determine the effect of the coating on certain aspects of the signaling pathway related to NRF2. We tested SiON<sub>x</sub> and further modified the structure with a small amount of phosphate to obtain SiONP<sub>x</sub> coatings (P/N = 0.1) to assess their effects associated with signaling and angiogenesis using MSCs and HUVECs. NRF2 is activated when it is translocated to the nucleus by Kelch-like ECH-associated protein (Keap1), where it separates and allows NRF2 to activate the downstream antioxidant signals [52]. This NRF2 activation is further enhanced by the presence of 2<sup>+</sup> or 4<sup>+</sup> cations [17,53,54]. In our first evaluation of PECVD SiON<sub>x</sub> coatings, we found that SiON<sub>x</sub> with N/O = 2 enhanced osteogenesis via SOD1-dependent activity [40,55]. We further observed that SiON<sub>x</sub> (with surface Si<sup>4+</sup>) spurred cytosolic NRF2 (Figure 14A) while Keap1 remained in the nucleus (Figure 14B).

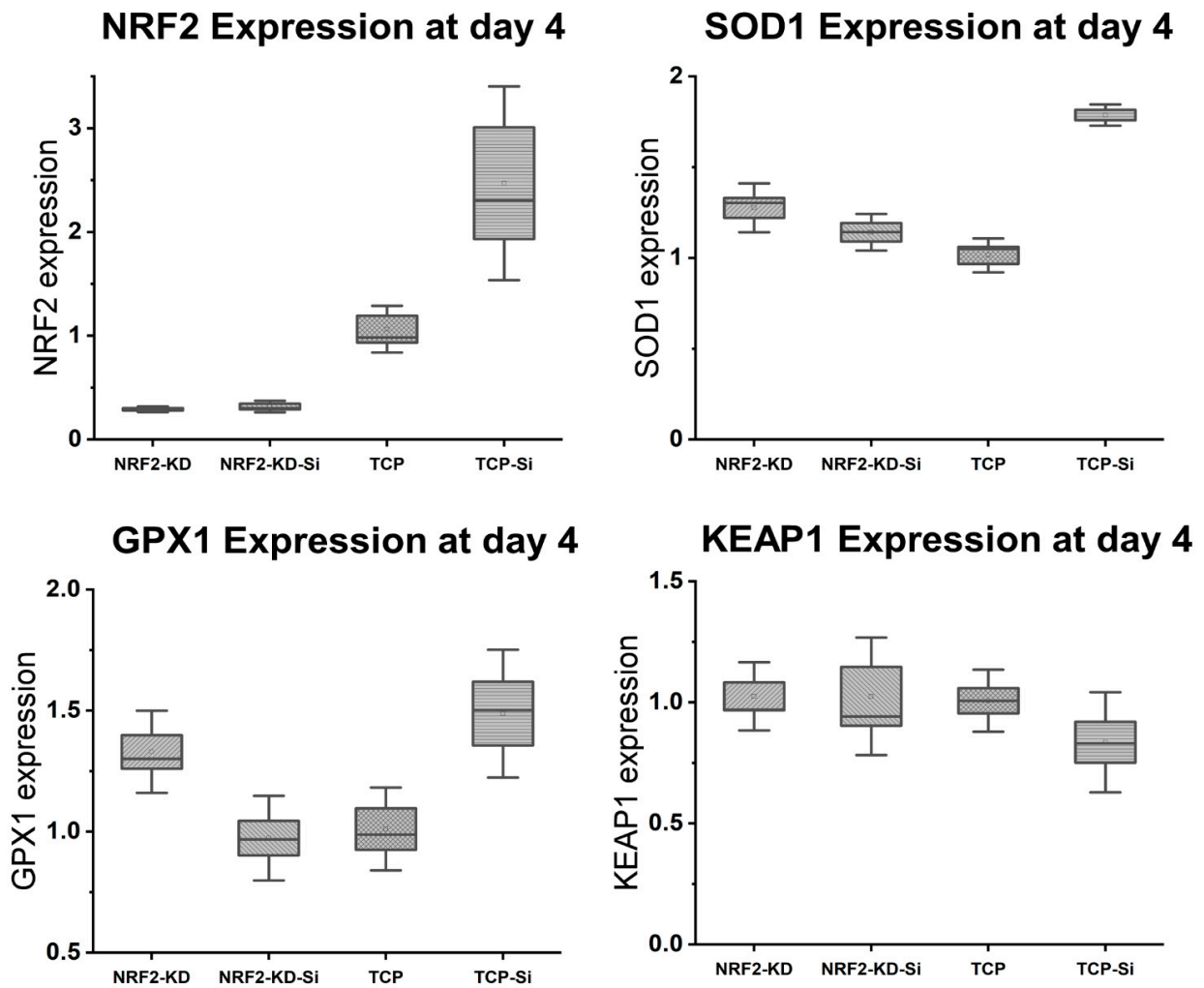


Figure 13. NRF2 KD blocks the Si ion protective effect on the antioxidant expression.

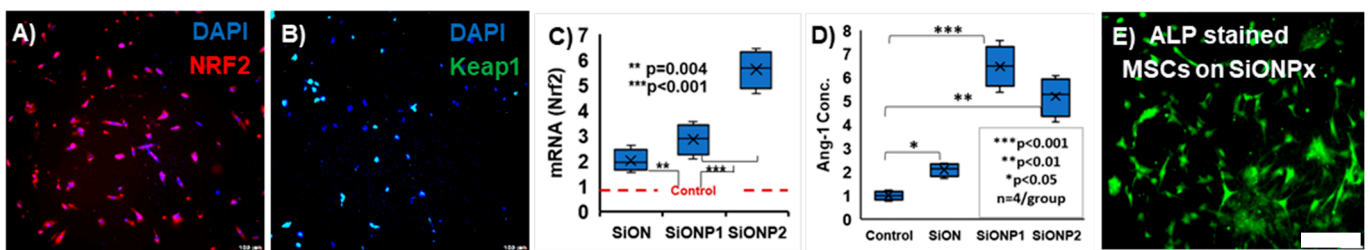
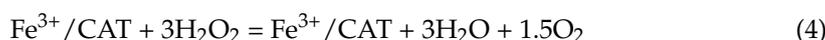
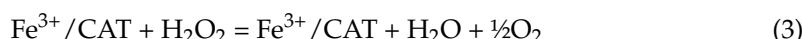
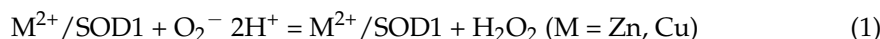


Figure 14. SiON<sub>x</sub> and SiONP<sub>x</sub> enhanced NRF2 and angiotensin (ANG1) vs. control. (A) DAPI (blue)/NRF2 (red): IHC image shows cytosolic NRF2 expression in MSCs (exposed to ROS) on SiON<sub>x</sub> coatings. NRF2 was stained with polyclonal anti-NRF2 Ab, followed by Alexa-594 secondary Ab, while the nucleus was counterstained with DAPI. (B) DAPI (blue)/Keap1 (green): IHC image shows nuclear localization of Keap1 in MSCs (exposed to ROS) on SiON<sub>x</sub> coatings. SiONP<sub>x</sub> (SiONP1: P/N = 0.9, SiONP2: P/N = 1.0) enhanced NRF2 activity (C) and ANG1 (D) vs. SiON<sub>x</sub>. (E) Alkaline phosphatase (ALP)-stained differentiated MSCs on SiONP<sub>x</sub>-Ti. \*  $p < 0.05$ , \*\*  $p < 0.01$ , \*\*\*  $p < 0.001$  present the significance compared to the control. Scale bar = 200  $\mu\text{m}$ .

In our previous reports [43,48], we noted that adding phosphate enhances HA formation and Si<sup>4+</sup> release. Thus, we added a small amount of phosphate to make SiONP<sub>x</sub> coatings (P/N = 0.1) [39]. When we increased the P/N ratio to 1.0 (Figure 14D), NRF2 and angiotensin increased in vitro (SiONP2, Figure 14C,D), as did the MSC alkaline phos-

phatase (ALP) activity (Figure 14E). Accordingly, our working hypotheses are as follows: (1) increased charge transfer from the surface  $\text{Si}^{4+}$  valence state catalyzes ROS reduction (Equations (1)–(4)); (2) surface  $\text{Si}^{4+}$  may enhance NRF2 activity due to Keap1 sensitivity to  $2^+$  and  $4^+$  cations [53], thereby allowing NRF2 release; and (3) an increased P/N ratio in  $\text{SiON}_x$  increases  $\text{Si}^{4+}$  surface ion release for the activation of these antioxidant signaling pathways. We will comprehensively explore the effect of P addition in  $\text{SiON}_x$  coatings as a part of our future studies.

**$\text{Si}^{4+}$  effect:** Equation (2) produces  $3\times$  more  $\text{H}_2\text{O}_2$  than Equation (1), which causes Equation (3) to produce more  $\text{H}_2\text{O} + \text{O}_2$  (Equation (4)).



#### 4. Discussion

In this study, we investigated the effect of increasing the nitrogen content in  $\text{SiON}_x$  surface coatings on bacterial growth and in vitro mesenchymal stem cell viability, proliferation, and osteogenic capacity. In addition, we examined the effect of the coatings on MSCs under hydrogen peroxide exposure inducing cellular-level oxidative stress.

Our results indicate that  $\text{SiON}_x$  coatings have a bacteriostatic effect, inhibiting bacterial growth and proliferation (Figure 1 and Supplemental Figure S1) as compared to a regular titanium surface. MRSA is the most common bacterial infection related to bone and joint injuries and is the most prevalent cause of hospital-acquired infections. As these  $\text{SiON}_x$  PECVD-based coatings are amorphous in nature [55], they have an ability to partially dissolve in the physiological environment and release Si ions as well as facilitate the formation of silanol surface groups ( $\text{Si}-\text{OH}$ ) similar to a bioactive glass surface [34,56,57]. It is known that bioactive glass stimulates various biological responses when immersed in physiological fluids, causing the exchange of network-modifier ions and  $\text{Si}-\text{OH}$  surface groups [56]. These surface changes activate mechanisms that efficiently inhibit bacterial growth and thus promote the adhesion and contamination of implants. We speculate that the  $\text{SiON}_x$  coatings have the same antibacterial effect. In the present study, increasing the nitrogen content in the  $\text{SiON}_x$  chemistry enhanced the coating's bacterial inhibition compared to the Ti surface and  $\text{SiON}_x$  with a low nitrogen content. Thus, the presented data suggest a possible antibacterial/bacteriostatic effect of  $\text{SiON}_x$  coatings compared to the Ti implants.

Reactive oxygen species (ROS) have been shown to play a role in aging and several pathological conditions, as well as traumatic injuries [58,59]. The role of ROS in bone metabolism is dual, considering its effects under physiological or pathological conditions [60]. Under physiological conditions, ROS production by osteoclasts helps accelerate the destruction of calcified tissue, assisting in bone remodeling. Under pathological conditions, such as bone fractures, pronounced radical generation occurs [4,5]. The inhibition of the activities of antioxidant enzymes, such as superoxide dismutase and glutathione peroxidase, was found to increase the production of superoxide by osteoclasts, leading to a delayed bone remodeling process [5]. Therefore, oxidative stress is an important mediator of bone remodeling and healing, whereas the compensatory antioxidant mechanism helps restore the physiological process [8,61]. Accordingly, increased free radical production overwhelms the natural antioxidant defense mechanisms, subjecting tissues to hyperoxidant stress and delaying bone healing. In addition, antioxidant administration might help in the acceleration of healing of fractured bones to some extent but does not guarantee a full physiological recovery in cases of large and compromised bone defects. Thus, biomaterials that can treat the defect by reducing ROS and stimulating osteogenesis within the bone defect can greatly improve the efficacy of such treatments in repairing the lost bone.

Under normal physiological *in vitro* conditions, we observed no significant differences in the various SiON<sub>x</sub>-coated surfaces as compared to a cell-culture-treated surface as a positive control, indicating favorable cellular viability and proliferation on the coated surfaces (Figure 3). Increasing the N/O ratio had a positive impact on the MSC osteogenic differentiation, manifesting as an increase in the ALP activity (Figure 4) and various other markers (Figures 5 and 6). When oxidative stresses were introduced to the physiological cell culture environment, we observed significant differences in the viability and proliferation of the mesenchymal stem cells with the increase in the N/O ratio in SiON<sub>x</sub>. Increasing the N/O ratio resulted in an increasing protective phenomenon (attributed to the change in charge) towards the mesenchymal stem cells with no significant differences in cell numbers when compared to cells grown in a normal physiological environment (Figure 8). Under oxidative stress conditions, we noted an upregulation of the osteogenic markers and antioxidant markers in the SiON<sub>x</sub> *n* = 1.82 group compared to the other groups. This upregulation was similar to the control with no oxidative stress conditions or even significantly higher for osteogenic markers such as ALPL and osteocalcin. As previously reported by our group [33], the Si–H and N–H bonds increase with the increase in N content in the Si–O–N structure. Moreover, the increased nitrogen reduces the partial charge of constituent elements and changes the bonding structure from random bonding to random mixing. We observed that SiON<sub>x</sub> with the refractive index of *n* = 1.82 enhances bioactivity and maximizes the antioxidant effect against the oxidative stresses, exhibiting [Si–Si]–[Si–O]–[Si–N] bonds as compared to SiON<sub>x</sub> *n* = 2 (which is nitrogen-rich, SiN<sub>x</sub>).

Several studies have shown that NRF2 is a key transcription factor that maintains homeostasis in bone cells, especially against oxidative stresses [41,62]. The findings yielded by these studies implicate the antioxidant pathway activation of NRF2 against detrimental oxidative stress along with the enhancement of osteogenesis in MSCs as being involved in the bone healing of fractures. NRF2 is also known to be of crucial importance in reducing the impact of degenerative bone diseases [63]. Under physiological conditions, NRF2 is negatively regulated by its cytoplasmic antagonist Keap1. However, ROS can deactivate Keap1 to prevent NRF2 degradation [37,63]. This leads to NRF2 being translocated and binding to ARE, which encodes antioxidant enzymes and cytoprotective proteins [11]. Our previous investigations demonstrated the expression of several antioxidants, including SOD1 and GPX, on endothelial cell lines [37]. In this study, we show the overexpression of NRF2 under oxidative stress conditions for SiON<sub>x</sub> (Figures 11 and 12) along with other antioxidant markers. When we blocked NRF2 (NRF2-KD), we did not observe the upregulation of the antioxidant markers with the silicon ions as before (Figure 13). Moreover, we observed the nuclear localization of Keap1 in MSCs cultured on the SiON<sub>x</sub> surface (Figure 14). These findings indicate that our initial assumption that SiON<sub>x</sub> induces the antioxidant properties through the NRF2 pathway is correct. We are of the view that this overexpression of NRF2 activity and relatively unaffected Keap1 activity (normalized to the cell number) (Figure 13 and Supplemental Figure S3) indicate the activation of the NRF2-ARE pathway to induce antioxidant enzymes and cytoprotective proteins along with enhancing osteogenic capacity in the MSCs.

Complicated bone defects can originate from a myriad of situations, as the “hidden” aspect of oxidative stress can manifest as a result of a patient’s biological conditions, such as diabetes or aging. Thus, biomaterials that can treat the defect by reducing ROS and stimulating osteogenesis for MSCs within the bone defect can greatly improve the efficacy of such treatments in repairing the lost bone.

In conclusion, the SiON<sub>x</sub> coatings examined as a part of this work displayed bacteriostatic properties and supported mesenchymal stem cell viability and proliferation. Increasing the nitrogen-to-oxygen ratio while keeping the silicon content constant led to an increase in osteogenic capacity under normal physiological conditions. When the NRF2 overexpression on the SiON<sub>x</sub> coatings with the highest N/O ratio was activated under toxic oxidative stress conditions, a protective antioxidant effect was observed, inducing ROS reduction and robust osteogenic marker expression and enhancing osteogenic capacity.

**Supplementary Materials:** The following supporting information can be downloaded at <https://www.mdpi.com/article/10.3390/antiox13020189/s1>: Figure S1.1: Bacteriostatic effect of SiONx coatings versus Ti implants. Fluorescence images show the live (green) and dead bacteria (red) on the different SiONx surfaces compared to Ti implant after 12 h. Figure S1.2: Bacteriostatic effect of SiONx coatings versus Ti implants. Fluorescence images show the live (green) and dead bacteria (red) on the different SiONx surfaces compared to Ti implant after 24 h. Figure S2: Live/dead assay performed after 4 days of an initial 24 h insult using various concentrations of hydrogen peroxide to study the sustained toxic effects of H<sub>2</sub>O<sub>2</sub> on MSCs. Figure S3: IHC staining representing DAPI and Keap1 on MSCs after 7 days of osteogenic differentiation. There is no significant difference in the Keap1 activity on the SiONx surface when compared to the control.

**Author Contributions:** Data curation, N.A. and K.A.; formal analysis, H.D. and S.Y. (Simon Young); funding acquisition, V.V.; investigation, N.A., K.A. and S.Y. (Su Yang); methodology, N.A. and K.A.; project administration, M.B. and V.V.; resources, H.D., S.Y. (Simon Young), P.A., M.B. and V.V.; validation, N.A.; writing—original draft, N.A.; writing—review and editing, K.A., P.A., A.M., S.Y. (Simon Young), M.B. and V.V. All authors have read and agreed to the published version of the manuscript.

**Funding:** This research was funded by the National Institutes of Health/National Institute of Dental and Craniofacial Research (NIH/NIDCR), grant numbers 1R01DE031872-01 and 1R56DE027964-01A1-01, and the APC was funded by 1R01DE031872-01. Also, funds were received from the Osteo Science Foundation Peter L. Geistlich Research Grant, Texas STARs award, Departmental Start-up Funds, and the University of Texas at Arlington (UTA) College of Nursing and Health Innovation, Arlington, TX. The following NIH Grants supported K.A. and M.B.: National Institutes of Aging (NIA) 7-PO1AG039355, NIA 5R01AG056504, and NIA 5R01AG060341; National Institutes of Neurological Disorders and Stroke (NINDS) 2-R01NS105621; National Institutes of Diabetes, Digestive, and Kidney Diseases Kidney NIDDK 5R01DK119066 to MB. NIA 7-PO1AG039355 partially supported this work.

**Institutional Review Board Statement:** Not applicable.

**Informed Consent Statement:** Not applicable.

**Data Availability Statement:** The data presented in this study are available on request from the corresponding author.

**Acknowledgments:** The authors would like to thank the UTA College of Nursing & Health Innovation-Bone-Muscle Research Center (UTA-CONHI-BMRC) and Nanotechnology Research Center at Shimadzu Center at UTA for their support. Lastly, we want to acknowledge Lauren Abbo Nono, a summer intern student in the Varanasi laboratory, for her contribution towards this study.

**Conflicts of Interest:** The authors declare no conflicts of interest.

## References

1. Dimitriou, R.; Jones, E.; McGonagle, D.; Giannoudis, P.V. Bone regeneration: Current concepts and future directions. *BMC Med.* **2011**, *9*, 66. [[CrossRef](#)]
2. Nauth, A.; Schemitsch, E.; Norris, B.; Nollin, Z.; Watson, J.T. Critical-Size Bone Defects: Is There a Consensus for Diagnosis and Treatment? *J. Orthop. Trauma* **2018**, *32*, S7–S11. [[CrossRef](#)]
3. Sandukji, A.; Al-Sawaf, H.; Mohamadin, A.; Alrashidi, Y.; Sheweita, S.A. Oxidative stress and bone markers in plasma of patients with long-bone fixative surgery: Role of antioxidants. *Hum. Exp. Toxicol.* **2010**, *30*, 435–442. [[CrossRef](#)]
4. Banfi, G.; Iorio, E.L.; Corsi, M.M. Oxidative stress, free radicals and bone remodeling. *Clin. Chem. Lab. Med.* **2008**, *46*, 1550–1555. [[CrossRef](#)]
5. Sheweita, S.A.; Khoshhal, K.I. Calcium Metabolism and Oxidative Stress in Bone Fractures: Role of Antioxidants. *Curr. Drug Metab.* **2007**, *8*, 519–525. [[CrossRef](#)]
6. Wang, Z.; Ehnert, S.; Ihle, C.; Schyschka, L.; Pscherer, S.; Nussler, N.C.; Braun, K.F.; Van Griensven, M.; Wang, G.; Burgkart, R. Increased Oxidative Stress Response in Granulocytes from Older Patients with a Hip Fracture May Account for Slow Regeneration. *Oxidative Med. Cell. Longev.* **2014**, *2014*, 819847. [[CrossRef](#)]
7. Lean, J.M.; Davies, J.T.; Fuller, K.; Jagger, C.J.; Kirstein, B.; Partington, G.A.; Urry, Z.L.; Chambers, T.J. A crucial role for thiol antioxidants in estrogen-deficiency bone loss. *J. Clin. Invest.* **2003**, *112*, 915–923. [[CrossRef](#)]
8. Zhou, Q.; Zhu, L.; Zhang, D.; Li, N.; Li, Q.; Dai, P.; Mao, Y.; Li, X.; Ma, J.; Huang, S. Oxidative Stress-Related Biomarkers in Postmenopausal Osteoporosis: A Systematic Review and Meta-Analyses. *Dis. Markers* **2016**, *2016*, 7067984. [[CrossRef](#)]

9. Mathy-Hartert, M.; Hogge, L.; Sanchez, C.; Deby-Dupont, G.; Crielaard, J.M.; Henrotin, Y. Interleukin-1 $\beta$  and interleukin-6 disturb the antioxidant enzyme system in bovine chondrocytes: A possible explanation for oxidative stress generation. *Osteoarthr. Cartil.* **2008**, *16*, 756–763. [[CrossRef](#)]
10. Simunovic, N.; Devereaux, P.J.; Bhandari, M. Surgery for hip fractures: Does surgical delay affect outcomes? *Indian J. Orthop.* **2011**, *45*, 27–32. [[CrossRef](#)]
11. Kubo, Y.; Wruck, C.J.; Fragoulis, A.; Drescher, W.; Pape, H.C.; Lichte, P.; Fischer, H.; Tohidnezhad, M.; Hildebrand, F.; Pufe, T.; et al. Role of Nrf2 in Fracture Healing: Clinical Aspects of Oxidative Stress. *Calcif. Tissue Int.* **2019**, *105*, 341–352. [[CrossRef](#)]
12. Sun, Y.-X.; Li, L.; Corry, K.A.; Zhang, P.; Yang, Y.; Himes, E.; Mihuti, C.L.; Nelson, C.; Dai, G.; Li, J. Deletion of Nrf2 reduces skeletal mechanical properties and decreases load-driven bone formation. *Bone* **2015**, *74*, 1–9. [[CrossRef](#)]
13. Jiang, T.; He, Y. Recent Advances in the Role of Nuclear Factor Erythroid-2-Related Factor 2 in Spinal Cord Injury: Regulatory Mechanisms and Therapeutic Options. *Front. Aging Neurosci.* **2022**, *14*, 851257. [[CrossRef](#)]
14. Silvestro, S.; Mazzon, E. Nrf2 Activation: Involvement in Central Nervous System Traumatic Injuries. A Promising Therapeutic Target of Natural Compounds. *Int. J. Mol. Sci.* **2023**, *24*, 199. [[CrossRef](#)]
15. Awad, K.; Ahuja, N.; Yacoub, A.S.; Brotto, L.; Young, S.; Mikos, A.; Aswath, P.; Varanasi, V. Revolutionizing bone regeneration: Advanced biomaterials for healing compromised bone defects. *Front. Aging* **2023**, *4*, 1217054. [[CrossRef](#)]
16. Sun, Y.-X.; Xu, A.-H.; Yang, Y.; Li, J. Role of Nrf2 in bone metabolism. *J. Biomed. Sci.* **2015**, *22*, 101. [[CrossRef](#)]
17. McMahan, M.; Swift, S.R.; Hayes, J.D. Zinc-binding triggers a conformational-switch in the cullin-3 substrate adaptor protein KEAP1 that controls transcription factor NRF2. *Toxicol. Appl. Pharmacol.* **2018**, *360*, 45–57. [[CrossRef](#)]
18. Iwai-Yoshida, M.; Shibata, Y.; Wurihan; Suzuki, D.; Fujisawa, N.; Tanimoto, Y.; Kamijo, R.; Maki, K.; Miyazaki, T. Antioxidant and osteogenic properties of anodically oxidized titanium. *J. Mech. Behav. Biomed. Mater.* **2012**, *13*, 230–236. [[CrossRef](#)]
19. Xue, T.; Attarilar, S.; Liu, S.; Liu, J.; Song, X.; Li, L.; Zhao, B.; Tang, Y. Surface Modification Techniques of Titanium and its Alloys to Functionally Optimize Their Biomedical Properties: Thematic Review. *Front. Bioeng. Biotechnol.* **2020**, *8*, 603072. [[CrossRef](#)]
20. Schmidt, A.H.; Swiontkowski, M.F. Pathophysiology of Infections After Internal Fixation of Fractures. *JAAOS-J. Am. Acad. Orthop. Surg.* **2000**, *8*, 285–291. [[CrossRef](#)]
21. Flemming, H.-C.; Wingender, J. The biofilm matrix. *Nat. Rev. Microbiol.* **2010**, *8*, 623–633. [[CrossRef](#)]
22. Arciola, C.R.; Campoccia, D.; Montanaro, L. Implant infections: Adhesion, biofilm formation and immune evasion. *Nat. Rev. Microbiol.* **2018**, *16*, 397–409. [[CrossRef](#)]
23. Farag, A.; Abdal-hay, A.; Han, P.; Ivanovski, S. Fabrication of 3D melt electrowriting multiphase scaffold with bioactive and osteoconductive functionalities for periodontal regeneration. *Ceram. Int.* **2023**, *49*, 8015–8021. [[CrossRef](#)]
24. Abdal-hay, A.; Sheikh, F.A.; Shmroukh, A.N.; Mousa, H.M.; Kim, Y.-K.; Ivanovski, S. Immobilization of bioactive glass ceramics @ 2D and 3D polyamide polymer substrates for bone tissue regeneration. *Mater. Des.* **2021**, *210*, 110094. [[CrossRef](#)]
25. Abdal-hay, A.; Gulati, K.; Fernandez-Medina, T.; Qian, M.; Ivanovski, S. In situ hydrothermal transformation of titanium surface into lithium-doped continuous nanowire network towards augmented bioactivity. *Appl. Surf. Sci.* **2020**, *505*, 144604. [[CrossRef](#)]
26. Xiang, E.; Gómez-Cerezo, M.N.; Ali, Y.; Ramachandra, S.S.; Yang, N.; Dargusch, M.; Moran, C.S.; Ivanovski, S.; Abdal-hay, A. Surface Modification of Pure Zinc by Acid Etching: Accelerating the Corrosion Rate and Enhancing Biocompatibility and Antibacterial Characteristics. *ACS Appl. Mater. Interfaces* **2022**, *14*, 22554–22569. [[CrossRef](#)]
27. Xia, L.; Xie, Y.; Fang, B.; Wang, X.; Lin, K. In situ modulation of crystallinity and nano-structures to enhance the stability and osseointegration of hydroxyapatite coatings on Ti-6Al-4V implants. *Chem. Eng. J.* **2018**, *347*, 711–720. [[CrossRef](#)]
28. Goller, G. The effect of bond coat on mechanical properties of plasma sprayed bioglass-titanium coatings. *Ceram. Int.* **2004**, *30*, 351–355. [[CrossRef](#)]
29. Montazerian, M.; Hosseinzadeh, F.; Migneco, C.; Fook, M.V.L.; Bairo, F. Bioceramic coatings on metallic implants: An overview. *Ceram. Int.* **2022**, *48*, 8987–9005. [[CrossRef](#)]
30. Narayanan, R.; Seshadri, S.K.; Kwon, T.Y.; Kim, K.H. Calcium phosphate-based coatings on titanium and its alloys. *J. Biomed. Mater. Res. Part B Appl. Biomater.* **2008**, *85*, 279–299. [[CrossRef](#)]
31. Sadowski, T.; Golewski, P. (Eds.) Protective Thermal Barrier Coatings. In *Loadings in Thermal Barrier Coatings of Jet Engine Turbine Blades: An Experimental Research and Numerical Modeling*; Springer: Singapore, 2016; pp. 5–11.
32. Oku, T.; Suganuma, K.; Wallenberg, L.R.; Tomsia, A.P.; Gomez-Vega, J.M.; Saiz, E. Structural characterization of the metal/glass interface in bioactive glass coatings on Ti-6Al-4V. *J. Mater. Sci. Mater. Med.* **2001**, *12*, 413–417. [[CrossRef](#)]
33. Gomez-Vega, J.M.; Saiz, E.; Tomsia, A.P.; Marshall, G.W.; Marshall, S.J. Bioactive glass coatings with hydroxyapatite and Bioglass® particles on Ti-based implants. 1. Processing. *Biomaterials* **2000**, *21*, 105–111. [[CrossRef](#)]
34. Saffarian Tousi, N.; Velten, M.F.; Bishop, T.J.; Leong, K.K.; Barkhordar, N.S.; Marshall, G.W.; Loomer, P.M.; Aswath, P.B.; Varanasi, V.G. Combinatorial effect of Si<sup>4+</sup>, Ca<sup>2+</sup>, and Mg<sup>2+</sup> released from bioactive glasses on osteoblast osteocalcin expression and biomineralization. *Mater. Sci. Eng. C* **2013**, *33*, 2757–2765. [[CrossRef](#)]
35. van Oirschot, B.A.J.A.; Alghamdi, H.S.; Närhi, T.O.; Anil, S.; Al Farraj Aldosari, A.; van den Beucken, J.J.J.P.; Jansen, J.A. In vivo evaluation of bioactive glass-based coatings on dental implants in a dog implantation model. *Clin. Oral Implant. Res.* **2014**, *25*, 21–28. [[CrossRef](#)]
36. Roy, M.; Bandyopadhyay, A.; Bose, S. Induction plasma sprayed nano hydroxyapatite coatings on titanium for orthopaedic and dental implants. *Surf. Coat. Technol.* **2011**, *205*, 2785–2792. [[CrossRef](#)]

37. do Monte, F.A.; Ahuja, N.; Awad, K.R.; Pan, Z.; Young, S.; Kim, H.K.W.; Aswath, P.; Brotto, M.; Varanasi, V.G. Silicon Oxynitrophosphide Nanoscale Coating Enhances Antioxidant Marker-Induced Angiogenesis During in vivo Cranial Bone-Defect Healing. *JBMR Plus* **2021**, *5*, e10425. [[CrossRef](#)]
38. Ilyas, A.; Odatsu, T.; Shah, A.; Monte, F.; Kim, H.K.W.; Kramer, P.; Aswath, P.B.; Varanasi, V.G. Amorphous Silica: A New Antioxidant Role for Rapid Critical-Sized Bone Defect Healing. *Adv. Healthc. Mater.* **2016**, *5*, 2199–2213. [[CrossRef](#)]
39. Ilyas, A.; Velton, M.; Shah, A.; Monte, F.; Kim, H.K.W.; Aswath, P.B.; Varanasi, V.G. Rapid Regeneration of Vascularized Bone by Nanofabricated Amorphous Silicon Oxynitrophosphide (SiONP) Overlays. *J. Biomed. Nanotechnol.* **2019**, *15*, 1241–1255. [[CrossRef](#)]
40. Monte, F.; Awad, K.R.; Ahuja, N.; Kim, H.; Aswath, P.; Brotto, M.; Varanasi, V.G. Amorphous Silicon Oxynitrophosphide Coated Implants Boost Angiogenic Activity of Endothelial Cells. *Tissue Eng. Part A* **2020**, *26*, 15–27. [[CrossRef](#)]
41. Varanasi, V.G.; Ilyas, A.; Velten, M.F.; Shah, A.; Lanford, W.A.; Aswath, P.B. Role of Hydrogen and Nitrogen on the Surface Chemical Structure of Bioactive Amorphous Silicon Oxynitride Films. *J. Phys. Chem. B* **2017**, *121*, 8991–9005. [[CrossRef](#)]
42. Tian, B.; Liu, Y. Antibacterial applications and safety issues of silica-based materials: A review. *Int. J. Appl. Ceram. Technol.* **2021**, *18*, 289–301. [[CrossRef](#)]
43. Awad, K.; Young, S.; Aswath, P.; Varanasi, V. Interfacial adhesion and surface bioactivity of anodized titanium modified with SiON and SiONP surface coatings. *Surf. Interfaces* **2022**, *28*, 101645. [[CrossRef](#)]
44. Yun, J.; Wang, W.; Kim, S.M.; Bae, T.-S.; Lee, S.; Kim, D.; Lee, G.-H.; Lee, H.-S.; Song, M. Light trapping in bendable organic solar cells using silica nanoparticle arrays. *Energy Environ. Sci.* **2015**, *8*, 932–940. [[CrossRef](#)]
45. Awad, K.; Ahuja, N.; Fiedler, M.; Peper, S.; Wang, Z.; Aswath, P.; Brotto, M.; Varanasi, V. Ionic Silicon Protects Oxidative Damage and Promotes Skeletal Muscle Cell Regeneration. *Int. J. Mol. Sci.* **2021**, *22*, 497. [[CrossRef](#)]
46. Pezzotti, G.; Bock, R.M.; McEntire, B.J.; Jones, E.; Boffelli, M.; Zhu, W.; Baggio, G.; Boschetto, F.; Puppulin, L.; Adachi, T.; et al. Silicon Nitride Bioceramics Induce Chemically Driven Lysis in *Porphyromonas gingivalis*. *Langmuir* **2016**, *32*, 3024–3035. [[CrossRef](#)]
47. Jensen, J.; Kraft, D.C.E.; Lysdahl, H.; Foldager, C.B.; Chen, M.; Kristiansen, A.A.; Rölfing, J.H.D.; Bünger, C.E. Functionalization of Polycaprolactone Scaffolds with Hyaluronic Acid and  $\beta$ -TCP Facilitates Migration and Osteogenic Differentiation of Human Dental Pulp Stem Cells In Vitro. *Tissue Eng. Part A* **2014**, *21*, 729–739. [[CrossRef](#)]
48. Ilyas, A.; Lavrik, N.V.; Kim, H.K.W.; Aswath, P.B.; Varanasi, V.G. Enhanced Interfacial Adhesion and Osteogenesis for Rapid “Bone-like” Biomineralization by PECVD-Based Silicon Oxynitride Overlays. *ACS Appl. Mater. Interfaces* **2015**, *7*, 15368–15379. [[CrossRef](#)]
49. Sandle, T. (Ed.) 6-Dry Heat Sterilisation. In *Sterility, Sterilisation and Sterility Assurance for Pharmaceuticals*; Woodhead Publishing: Cambridge, UK, 2013; pp. 83–92.
50. Rose, J.; Vaughan, J. In Vitro Test Methods for Antimicrobial Coatings on Medical Devices: Learnings from Industry. In *Antimicrobial Combination Devices*; Urish, K.L., Mihalko, W.M., Eds.; ASTM International: West Conshohocken, PA, USA, 2020; pp. 38–52.
51. Tong Steven, Y.C.; Joshua, S.D.; Eichenberger, E.; Thomas, L.H.; Vance, G.F. Staphylococcus aureus Infections: Epidemiology, Pathophysiology, Clinical Manifestations, and Management. *Clin. Microbiol. Rev.* **2015**, *28*, 603–661. [[CrossRef](#)]
52. Velichkova, M.; Hasson, T. Keap1 regulates the oxidation-sensitive shuttling of Nrf2 into and out of the nucleus via a Crm1-dependent nuclear export mechanism. *Mol. Cell. Biol.* **2005**, *25*, 4501–4513. [[CrossRef](#)]
53. Tebay, L.E.; Robertson, H.; Durant, S.T.; Vitale, S.R.; Penning, T.M.; Dinkova-Kostova, A.T.; Hayes, J.D. Mechanisms of activation of the transcription factor Nrf2 by redox stressors, nutrient cues, and energy status and the pathways through which it attenuates degenerative disease. *Free Radic. Biol. Med.* **2015**, *88 Pt B*, 108–146. [[CrossRef](#)]
54. Dinkova-Kostova, A.T.; Holtzclaw, W.D.; Wakabayashi, N. Keap1, the Sensor for Electrophiles and Oxidants that Regulates the Phase 2 Response, Is a Zinc Metalloprotein. *Biochemistry* **2005**, *44*, 6889–6899. [[CrossRef](#)]
55. Varanasi, V.G.; Velten, M.F.; Odatsu, T.; Ilyas, A.; Iqbal, S.M.; Aswath, P.B. Surface Modifications and Surface Characterization of Biomaterials Used in Bone Healing. In *Materials and Devices for Bone Disorders*; Academic Press: Cambridge, MA, USA, 2016; pp. 405–452.
56. Drago, L.; Toscano, M.; Bottagisi, M. Recent Evidence on Bioactive Glass Antimicrobial and Antibiofilm Activity: A Mini-Review. *Materials* **2018**, *11*, 326. [[CrossRef](#)]
57. Odatsu, T.; Azimaie, T.; Velten, M.F.; Vu, M.; Lyles, M.B.; Kim, H.K.; Aswath, P.B.; Varanasi, V.G. Human periosteum cell osteogenic differentiation enhanced by ionic silicon release from porous amorphous silica fibrous scaffolds. *J. Biomed. Mater. Res. Part A* **2015**, *103*, 2797–2806. [[CrossRef](#)] [[PubMed](#)]
58. Jelic, M.D.; Mandic, A.D.; Maricic, S.M.; Srdjenovic, B.U. Oxidative stress and its role in cancer. *J. Cancer Res. Ther.* **2021**, *17*, 22–28. [[CrossRef](#)]
59. Förstermann, U.; Sessa, W.C. Nitric oxide synthases: Regulation and function. *Eur. Heart J.* **2012**, *33*, 829–837. [[CrossRef](#)]
60. Basu, S.; Michaëlsson, K.; Olofsson, H.; Johansson, S.; Melhus, H. Association between Oxidative Stress and Bone Mineral Density. *Biochem. Biophys. Res. Commun.* **2001**, *288*, 275–279. [[CrossRef](#)] [[PubMed](#)]
61. Liu, W.; Chen, D.; Jiang, G.; Li, Q.; Wang, Q.; Cheng, M.; He, G.; Zhang, X. A lithium-containing nanoporous coating on entangled titanium scaffold can enhance osseointegration through Wnt/ $\beta$ -catenin pathway. *Nanomed. Nanotechnol. Biol. Med.* **2018**, *14*, 153–164. [[CrossRef](#)] [[PubMed](#)]

62. Lippross, S.; Beckmann, R.; Streubesand, N.; Ayub, F.; Tohidnezhad, M.; Campbell, G.; Kan, Y.W.; Horst, F.; Sönmez, T.T.; Varoga, D. Nrf2 Deficiency Impairs Fracture Healing in Mice. *Calcif. Tissue Int.* **2014**, *95*, 349–361. [[CrossRef](#)]
63. Sies, H. Hydrogen peroxide as a central redox signaling molecule in physiological oxidative stress: Oxidative eustress. *Redox Biol.* **2017**, *11*, 613–619. [[CrossRef](#)]

**Disclaimer/Publisher’s Note:** The statements, opinions and data contained in all publications are solely those of the individual author(s) and contributor(s) and not of MDPI and/or the editor(s). MDPI and/or the editor(s) disclaim responsibility for any injury to people or property resulting from any ideas, methods, instructions or products referred to in the content.